Electron spillover effects in In Ga N Ga N quantum-well lasers

Shyh-Jer Huang and Shun-Tung Yen

Citation: Journal of Applied Physics **102**, 113112 (2007); doi: 10.1063/1.2821411
View online: http://dx.doi.org/10.1063/1.2821411
View Table of Contents: http://scitation.aip.org/content/aip/journal/jap/102/11?ver=pdfcov
Published by the AIP Publishing

Electron spillover effects in InGaN/GaN quantum-well lasers

Shyh-Jer Huang and Shun-Tung Yen[a)]
Department of Electronics Engineering, National Chiao Tung University, Hsinchu, Taiwan 30050, Republic of China

(Received 29 May 2007; accepted 13 October 2007; published online 10 December 2007)

The effects of electron spillover from quantum wells on the optical property of InGaN/GaN laser diodes are theoretically studied in detail. A six-band model including strain effects is used to calculate valence band states. Continuous subbands unconfined to the quantum wells are simulated deliberately by densely discretized subbands for the spillover electrons. The calculation results show obvious differences in the radiative current densities and the gain spectra between the cases with and without considering the spillover effect. We further investigate the spillover effect on the radiative current densities and the spontaneous emission spectra, with variations in the depth and the width of quantum wells, the total loss of the cavity, and the temperature. For shallow wells, the spillover effect is particularly important. It broadens both the gain and the spontaneous emission spectra and hence deteriorates the threshold of laser diodes. Such an effect can be alleviated by employing a long cavity and a multi-quantum-well active region. The concept of the electron spillover studied in this work is not only applicable to the nitride lasers but also to other kinds of quantum-well lasers.
 [DOI: 10.1063/1.2821411]

I. INTRODUCTION

In recent years there has been a lot of research effort in exploring blue-violet light sources, such as light-emitting diodes (LEDs) and laser diodes (LDs), due to their potential applications in full-color displays and high-density optical storage. Potential materials for the short-wavelength emission include SiC-,[1] ZnSe-,[2,3] and GaN-based wide-gap semiconductors.[4] Among them, the nitrides, such as GaN and the related ternary (AlGaN and InGaN) and quaternary (AlGaInN) compounds, are considered more promising for high-brightness emission, and currently they have been used commercially in making up blue-violet and green LEDs and LDs. However, the reliability of the wide-gap nitride LDs is still an important issue because of their short lifetime caused by high threshold current. In comparison with conventional zinc-blende GaAs-based lasers, the high threshold current of the wurtzite nitride lasers may be attributed to several factors, including immature material preparation, the intrinsic large density of states in the valence bands, and large leakage current in the device structures not yet optimized.

The leakage current can be regarded as composed mainly of three components according to their different origins: (1) the component caused by nonradiative recombination of electrons and holes in the active region, (2) the one due to electron leakage from the active region to the *p*-type cladding layers,[5] and (3) the one caused by the interband transition of high-energy carriers in the neighborhood of the active region.[5] The leakage current due to nonradiative recombination has been considerably alleviated in the GaN lasers by the reduction of defects with the progress of material growth and device processing technologies.[6,7] As to the electron leakage into the *p*-type cladding layer, it has been commonly found from recent works that such leakage can be reduced significantly by the insertion of an AlGaN electron blocking layer (EBL) between the active region and the *p*-type layer.[8–12] Furthermore, it has been demonstrated that this leakage can be made very low compared to other leakages by optimization on the structure with EBL.[9–12] The hole leakage out of the active region can be neglected because of the large effective mass of the inertial holes. The EBL, however, cannot suppress the spillover of energetic carriers into the continuous subband states above the barriers in energy surrounding the quantum wells (QWs) of the active region. Interband transition involving the high-energy spillover carriers usually gives a negligibly small contribution to the optical peak gain of the QW active region but may cause significant consumption of electric current. Therefore, the recombination of spillover carriers can be regarded as one of the paths for the leakage current. Such a problem of carrier spillover depends on temperature and is particularly serious for electrons in the conduction bands because of the small electron effective mass, the large asymmetry between the densities of states of the conduction and valence bands, and the narrow QWs usually used in the nitride LDs. There are quite few literatures discussing leakage due to the recombination of spillover carriers,[5] and so far, the influences of the optical transitions from the spillover carriers on the shapes of gain and spontaneous emission spectra have not been discussed and analyzed in detail. Furthermore, there has not been any research work on this problem for the short-wavelength nitride LDs.

In this paper, we present the calculation results of the carrier spillover effects on the optical gain, the spontaneous emission, and the threshold current for InGaN/GaN QW LDs. The calculation is based on the six-band model for the valence band states. Continuous subbands above the barriers in energy are deliberately treated for the spillover carriers. We found that the electron spillover can broaden the gain and

[a)]Electronic mail: styen@mail.nctu.edu.tw.

the spontaneous emission spectra, deteriorating the threshold of QW LDs. A multi-QW structure is then proposed to solve the problem.

This paper is organized as follows. The calculation approaches are described in the following section. We then present our calculation results with detailed discussion in Sec. III. Finally, we draw the conclusion in Sec. IV.

II. CALCULATION APPROACHES

We consider the wurtzite III-nitride lasers with a conventional step separate-confinement heterostructure that contains an undoped active region of strained InGaN/GaN QWs and is inserted with an AlGaN EBL immediately near the QWs.[10] The layers are considered to be grown on strain-free GaN along the crystallographic *c*-axis which is defined as the *z*-axis. We take the flatband approximation to calculate the band structure of the QWs. This is a good approximation for narrow QWs considered in this study, even if the strain-induced piezoelectric field in the InGaN QWs may be considerable.[13] At threshold condition, the piezoelectric field is strongly suppressed by the screening of the large density of carriers (generally in the range of $10^{19}-10^{20}$ cm^{-3}), further justifying the flatband approximation. It has also been pointed out that, in this range of threshold carrier density, there is a small difference from the case of full screening in the transition energy and the recombination rate between the lowest conduction and valence subbands.[14] Franssen *et al.* have experimentally demonstrated that the polarization-induced electric field can be almost fully screened in nitride LDs close to lasing threshold, supporting our assumption of the flatband approximation.[15]

The valence band structure of the InGaN/GaN QWs is calculated based on the six-band $\mathbf{k}\cdot\mathbf{p}$ model which includes the coupling of the heavy-hole, the light-hole, and the spin-orbit split-off bands.[16,17] The strain effect is also included in this model. By means of a unitary transformation of basis functions, the 6×6 Hamiltonian in the six-band model can be block diagonalized into one consisting of two 3×3 blocks,[17]

$$\hat{H}(\hat{k}_z;k_t)=\begin{bmatrix}\hat{H}^{+}(\hat{k}_z;k_t) & 0\\ 0 & \hat{H}^{-}(\hat{k}_z;k_t)\end{bmatrix}, \tag{1}$$

with

$$\hat{H}^{\pm}=\begin{bmatrix}\hat{F} & K_t & \mp i\hat{H}_t\\ K_t & \hat{G} & \Delta\mp i\hat{H}_t\\ \pm i\hat{H}_t^{\dagger} & \Delta\pm i\hat{H}_t^{\dagger} & \hat{\lambda}\end{bmatrix}, \tag{2}$$

$$\hat{F}=\Delta_1+\Delta_2+\hat{\lambda}+\hat{\theta},$$

$$\hat{G}=\Delta_1-\Delta_2+\hat{\lambda}+\hat{\theta},$$

$$\hat{\lambda}=\frac{\hbar^2}{2m_0}(\hat{k}_zA_1\hat{k}_z+A_2k_t^2)+D_1\epsilon_{\perp}+2D_2\epsilon_{\parallel},$$

$$\hat{\theta}=\frac{\hbar^2}{2m_0}(\hat{k}_zA_3\hat{k}_z+A_4k_t^2)+D_3\epsilon_{\perp}+2D_4\epsilon_{\parallel},$$

$$K_t=\frac{\hbar^2}{2m_0}A_5k_t^2,$$

$$\hat{H}_t=\frac{\hbar^2}{2m_0}\frac{k_t}{\sqrt{2}}[\hat{k}_z(1+\sqrt{2}A_6-A_1-A_3)-(1-A_1-A_3)\hat{k}_z],$$

$$\Delta=\sqrt{2}\Delta_3, \quad \text{and } \hat{k}_z=-i\partial/\partial z, \tag{3}$$

where m_0 is the free electron mass and $k_t=\sqrt{k_x^2+k_y^2}$ is the magnitude of the in-plane wave vector. The parameters $\Delta_i(i=1-3)$ account for either the crystal-field split energy (Δ_1) or the spin-orbit interactions (Δ_2 and Δ_3). The $A_i(i=1-6)$ are effective-mass-like parameters and the $D_i(i=1-4)$ are deformation potential constants. The normal strain components $\epsilon_{\perp}$ and $\epsilon_{\parallel}$ in the QW region are given by

$$\epsilon_{\parallel}=\frac{a_0-a}{a} \text{ and } \epsilon_{\perp}=-\frac{2C_{13}}{C_{33}}\epsilon_{\parallel}, \tag{4}$$

where a_0 and a are the lattice constants of undeformed materials making up the substrate and the QWs, which in the present study are GaN and InGaN, respectively. C_{13} and C_{33} are stiffness constants of the QW material.

Based on the $\mathbf{k}\cdot\mathbf{p}$ model, the wave functions of valence band states can be expressed as

$$\Psi^{\pm}(\mathbf{r};\mathbf{k}_t)=\frac{1}{\sqrt{A}}e^{i\mathbf{k}_t\cdot\mathbf{r}_t}\sum_{\mu=1}^{3}\psi_{\mu}^{\pm}(\hat{k}_z;k_t)u_{\mu}^{\pm}, \tag{5}$$

which, together with their energy E, can be solved by the effective-mass equation,

$$\sum_{\nu=1}^{3}[\hat{H}_{\mu\nu}^{\pm}(\hat{k}_z;k_t)+E_v^0(z)\delta_{\mu\nu}]\psi_{\nu}^{\pm}=E\psi_{\mu}^{\pm}, \quad \mu=1,2,3, \tag{6}$$

where the $\psi_{\mu}^{\pm}$ are envelope functions and the $u_{\mu}^{\pm}$ are the transformed basis functions according to which the Hamiltonians $\hat{H}_{\mu\nu}^{\pm}$ are built up;[16,17] A is the area of the QWs; $\mathbf{r}_t$ and $\mathbf{k}_t$ are the in-plane position vector and the wave vector of the particle, respectively; $E_v^0(z)$ is the z-dependent valence band edge of the undeformed materials composing the heterostructure. It is noticed that the order of the operators in Eq. (3) is of importance to the correct boundary conditions for matching the envelope functions.[17]

For the conduction band states, we use the single-band effective-mass equation,

$$\left[-\frac{\partial}{\partial z}\frac{\hbar^2}{2m_z}\frac{\partial}{\partial z}+\frac{\hbar^2k_t^2}{2m_t}+E_c^0(z)+a_{cz}\epsilon_{\perp}+2a_{ct}\epsilon_{\parallel}\right]\varphi=E\varphi, \tag{7}$$

to solve the envelope function φ and the energy E, where m_z (m_t) is the electron effective mass in the direction along (transverse to) the growth direction; $E_c^0(z)$ is the z-dependent conduction band edge of the undeformed materials composing the heterostructure; a_{cz} and a_{ct} are the deformation potentials for the conduction bands along and transverse to the

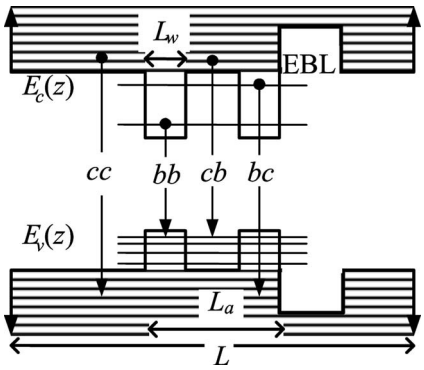

FIG. 1. Schematic illustration of the band diagram of the neighborhood of the InGaN/GaN QW active region inside which four different kinds (*bb*, *cb*, *bc*, and *cc*) of interband processes occur. The *cb* (*bb*) process means the interband process between the continuous (bound) conduction and the bound valence subbands while the *bc* (*cc*) means the process between the bound (continuous) conduction and the continuous valence subbands. The well has a width L_w and the active region has a width L_a. The continuous subbands are simulated by dense discrete subbands that are discretized using two infinite potential boundaries. An AlGaN EBL is placed immediately near the active region.

c-axis, respectively. Neglecting the small spin-splitting effect, we can write down the wave functions of conduction band states for spin up and spin down as simply a product of the envelope part and the Bloch function part,

$$\Phi^{\pm}(\mathbf{r};\mathbf{k}_t) = \frac{1}{\sqrt{A}} e^{i\mathbf{k}_t\cdot\mathbf{r}_t}\varphi(z;k_t)u_c^{\pm}, \tag{8}$$

where $u_c^{\pm}$ are the conduction band Bloch functions at the Γ point for spin up (+) and spin down (−).

Besides the discrete subbands bound by the barriers, we also consider the spillover of carriers to the continuous subband states which are above at least one side of the potential barriers in energy. We obtain the wave functions and the energy of the continuous subband states also using Eqs. (5)–(8), similar to the bound subband states, except that we use two infinite boundaries at positions sufficiently far away from each other for the continuous subbands, as illustrated in Fig. 1, where we include the EBL in the structure. Consequently, we obtain discrete subbands dense enough to realistically simulate the physical property of the real continuous subbands. Such infinite boundaries have been employed for the calculation of the continuous subband states in previous articles.[5,18] Justification and detailed discussion for the infinite boundaries can be found there.

To calculate the gain spectrum of the active region as a function of the carrier concentration, we assume that the electrons and the holes are in quasiequilibrium in the conduction bands and the valence bands, respectively, and that the electron sheet density is equal to the hole sheet density in the active region. It is therefore possible to determine the conduction band quasi-Fermi level F_c and the valence band quasi-Fermi level F_v for a given sheet carrier density n_a in the active region by the integrals

$$n_a = 2\sum_i \int P_i^c(k_t) f_i^c(F_c,k_t)\frac{k_t}{2\pi}dk_t$$

$$= \sum_{\sigma=\pm}\sum_j \int P_j^{\sigma}(k_t)[1-f_j^{\sigma}(F_v,k_t)]\frac{k_t}{2\pi}dk_t, \tag{9}$$

where the factor 2 in Eq. (9) accounts for the spin degeneracy in the conduction band. The functions $f_i^c(F_c,k_t)$ and $f_j^{\sigma}(F_v,k_t)$ are the Fermi-Dirac distribution functions for the probabilities of electrons occupying the states $\Phi_i^{\pm}(\mathbf{r};\mathbf{k}_t) = (1/\sqrt{A})e^{i\mathbf{k}_t\cdot\mathbf{r}_t}\varphi_i(z;k_t)u_c^{\pm}$ of conduction subband *i* and the state $\Psi_j^{\sigma}(\mathbf{r};\mathbf{k}_t) = (1/\sqrt{A})e^{i\mathbf{k}_t\cdot\mathbf{r}_t}\Sigma_{\mu=1}^{3}\psi_{\mu j}^{\sigma}(\hat{k}_z;k_t)u_{\mu}^{\sigma}$ of valence subband *j*, respectively; $P_i^c(k_t)$ and $P_j^{\sigma}(k_t)$ are the probabilities of finding the carriers at states $\Phi_i^{\pm}(\mathbf{r};\mathbf{k}_t)$ and $\Psi_j^{\sigma}(\mathbf{r};\mathbf{k}_t)$, respectively, in the active region with width L_a and can thus be expressed by

$$P_i^c(k_t) = \int_{L_a} |\varphi_i(z;k_t)|^2 dz,$$

$$P_j^{\sigma}(k_t) = \sum_{\mu=1}^{3}\int_{L_a} |\psi_{\mu j}^{\sigma}(\hat{k}_z;k_t)|^2 dz. \tag{10}$$

For a given sheet carrier concentration, the optical gain $g(\hbar\omega)$ and the spontaneous emission rate $r_{\mathrm{sp}}(\hbar\omega)$ are then calculated using the formulas[19]

$$g(\hbar\omega) = [1-e^{[\hbar\omega-(F_c-F_v)]/k_BT}]\sum_{ij} g_{\mathrm{sp},ij}^{e}(\hbar\omega), \quad e=x,y,z, \tag{11}$$

$$r_{\mathrm{sp}}(\hbar\omega) = \sum_{ij} r_{\mathrm{sp},ij}(\hbar\omega), \tag{12}$$

$$g_{\mathrm{sp},ij}^{e}(\hbar\omega) = \frac{2q^2\pi}{n_r c\epsilon_0 m_0^2\omega L_{ij}}\sum_{\sigma=\pm}\int |M_{e,ij}^{\sigma}|^2 \frac{f_i^c(1-f_j^{\sigma})\gamma/\pi}{(E_{ij}^{\sigma}-\hbar\omega)^2+\gamma^2} \times\frac{k_t}{2\pi}dk_t, \tag{13}$$

$$r_{\mathrm{sp},ij}(\hbar\omega) = \frac{n_r^2\omega^2}{\pi^2\hbar c^2}\frac{2g_{\mathrm{sp},ij}^{x}+g_{\mathrm{sp},ij}^{z}}{3}, \tag{14}$$

where ω is the angular frequency of the photon, T is the temperature, the superscript e is used to specify the polarization of the optical electric field, n_r is the averaged refractive index of the materials constituting the active region, q is the elementary charge, and ϵ_0 and c are the permittivity and the speed of light in vacuum, respectively; $E_{ij}^{\sigma} \equiv E_i^c(k_t) - E_j^{\sigma}(k_t)$ is the interband transition energy between the conduction subband state $\Phi_i^{+}(\mathbf{r};\mathbf{k}_t)$ [or $\Phi_i^{-}(\mathbf{r};\mathbf{k}_t)$] with energy $E_i^c(k_t)$ and the valence subband state $\Psi_j^{\sigma}(\mathbf{r};\mathbf{k}_t)$ with energy $E_j^{\sigma}(k_t)$. L_{ij} is the width of the region in which the interband process occurs between conduction subband *i* and valence subband *j*. Obviously, if both the subbands *i* and *j* are continuous, $L_{ij}=L$; otherwise, $L_{ij}=L_a$. γ^{-1} is the intraband relaxation time which we assume to be 0.1 ps. $M_{e,ij}^{\sigma}$ is the *e*-component of the momentum-matrix element for interband transition between

the states $\Phi_i^+(\mathbf{r};\mathbf{k}_t)$ [or $\Phi_i^-(\mathbf{r};\mathbf{k}_t)$] and $\Psi_j^\sigma(\mathbf{r};\mathbf{k}_t)$, with a modulus squared given by[19]

$$|M_{x,ij}^\sigma|^2 = |M_{y,ij}^\sigma|^2 = \frac{m_0 E_{px}}{8} \sum_{\mu=1,2} |\langle \varphi_i | \psi_{\mu j}^\sigma \rangle|^2, \tag{15}$$

for the TE-polarization component, and

$$|M_{z,ij}^\sigma|^2 = \frac{m_0 E_{pz}}{4} |\langle \varphi_i | \psi_{\mu=3,j}^\sigma \rangle|^2, \tag{16}$$

for the TM-polarization component, where the parameters E_{px} and E_{pz} are defined as

$$E_{px} = \left(\frac{m_0}{m_t} - 1\right) E_g \frac{(E_g + \Delta_1 + \Delta_2)(E_g + 2\Delta_2) - 2\Delta_3^2}{(E_g + \Delta_1 + \Delta_2)(E_g + \Delta_2) - \Delta_3^2},$$
$$E_{pz} = \left(\frac{m_0}{m_z} - 1\right) \frac{(E_g + \Delta_1 + \Delta_2)(E_g + 2\Delta_2) - 2\Delta_3^2}{E_g + 2\Delta_2}. \tag{17}$$

The component $r_{\mathrm{sp},ij}$ of the spontaneous emission rate is due to the recombination of electrons in conduction subband i and holes in valence subband j. It has the meaning of the number of emitting photons due to the recombinations per unit time per unit volume per unit photon energy interval at energy $\hbar\omega$. Accordingly, the corresponding component of the resulting radiative recombination current density can be written as

$$J_{ij} = qL_{ij} \int r_{\mathrm{sp},ij}(\hbar\omega) d\hbar\omega. \tag{18}$$

The total current density $J = \Sigma_{ij} J_{ij}$, which is the sum of all current density components J_{ij}, can also be considered as composed of four components, $J = J_{bb} + J_{bc} + J_{cb} + J_{cc}$. As illustrated in Fig. 1, the component J_{bb} is caused by the transitions from all the bound conduction subbands to all the bound valence subbands, the J_{bc} one is caused by the transitions from all the bound conduction subbands to all the continuous valence subbands, and J_{cb} (J_{cc}) is caused by the transitions from all the continuous conduction subbands to all the bound (continuous) valence subbands. These current components can be obtained by

$$J_{bb} = \sum_i^b \sum_j^b J_{ij}, \quad J_{bc} = \sum_i^b \sum_j^c J_{ij}$$
$$J_{cb} = \sum_i^c \sum_j^b J_{ij}, \quad \text{and } J_{cc} = \sum_i^c \sum_j^c J_{ij}, \tag{19}$$

where the symbols b and c over the sigmas mean summations over bound subbands and continuous subbands, respectively. For convenience in later analysis, the optical gain g and the spontaneous emission r_{sp} rate are also considered as composed of four components ($g = g_{bb} + g_{bc} + g_{cb} + g_{cc}$ and $r_{\mathrm{sp}} = r_{\mathrm{sp},bb} + r_{\mathrm{sp},bc} + r_{\mathrm{sp},cb} + r_{\mathrm{sp},cc}$) with their expressions similar to Eq. (19). It has been mentioned above that the electron leakage into the p-type cladding layer can be alleviated by the employment of EBL. Moreover, the main interest here is the investigation on the radiative current density involving the transitions from the continuous states, so the electron leakage over the EBL is ignored through this work. As for the leakage due to the nonradiative current, it relies on the material quality and processing technologies, and hence we skip this issue.

We are mainly interested in the effects of carrier spillover on threshold. For the threshold condition, we use the formula

$$\Gamma \max_{\hbar\omega} g(\hbar\omega) = \alpha, \tag{20}$$

where α is the cavity loss, Γ is the optical confinement factor, and $\max_{\hbar\omega} g(\hbar\omega)$ is the peak gain. From condition (20), we first obtain the quasi-Fermi levels, F_c and F_v, at threshold. With F_c and F_v, we obtain the carrier distribution in energy space, based on which we further calculate the gain spectra, the spontaneous emission rates, and the recombination current densities at threshold.

III. RESULTS AND DISCUSSION

In this section we present the calculated results and detailed analysis of the optical gains, the spontaneous emission, and the recombination current densities for $In_{0.2}Ga_{0.8}N/GaN$ QW lasers inserted with a 20 nm $Al_{0.2}Ga_{0.8}N$ EBL under the influence of the carrier spillover. All the values of the material parameters used in our calculation can be found from Ref. 20 for wurtzite GaN, InN, and AlN. The values for the ternary compounds InGaN and AlGaN are obtained by linear interpolation between the binary compounds, except for the band gap energy for which a bowing parameter of 1.4 eV is used for InGaN and that of 0.7 eV for AlGaN.[20] The band offset is a factor important in studying the spillover of carriers from the bound subbands. Unfortunately, till now there have been no compelling unambiguous values for the band offset of the nitride heterointerfaces. We thus take the valence band offset (VBO) ΔE_v or equivalently the valence band partition ratio Q_v as a variable parameter, where $\Delta E_v = Q_v \Delta E_g$ (ΔE_g is the band gap difference), and investigate the dependence of carrier spillover on the band offset. In the determination of the threshold condition, we assume that the lasers have structures such that the confinement factor $\Gamma = 3 \times 10^{-4} L_a$, where L_a is the active region width in units of angstroms. This gives $\Gamma = 1.5\%$ for a 50 Å QW, a value reasonable for typical III-nitride LDs. The total loss of the cavity is set at $\alpha = 60\ \mathrm{cm}^{-1}$ for the threshold condition [Eq. (20)] except in the case where the loss α is considered as a variable parameter. The temperature is set at $T = 300$ K except in the case where we investigate the dependence of carrier spillover on temperature.

The density of carriers at threshold in our calculation is in the range from 2×10^{19} to $6 \times 10^{19}\ \mathrm{cm}^{-3}$, depending on the well width, the cavity loss, and the temperature. At the high carrier concentration, it is feasible to employ the flat-band approximation in studying the effects of carrier spillover for InGaN laser diodes here.

Figure 2 shows the current densities, J, J_{bb}, and J_0, versus the peak gain for single-QW structures with well widths $L_w = 3.6$ and 5.4 nm, assuming the partition ratios $Q_v = 0.33$ in panel (a) and $Q_v = 0.45$ in panel (b). Here, for comparison, we include the current density J_0 which is calculated without

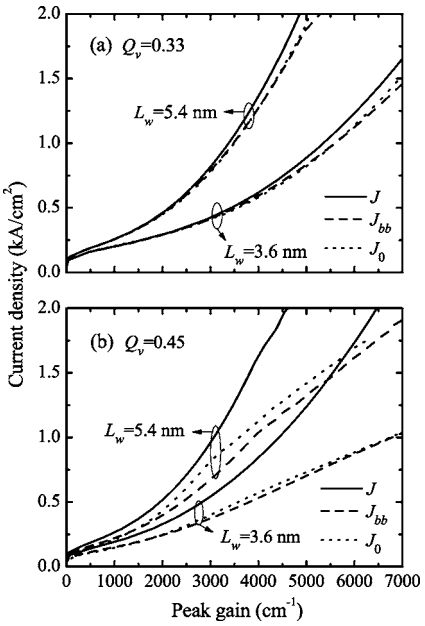

FIG. 2. The current densities, J, J_{bb}, and J_0, vs the peak gain for $In_{0.2}Ga_{0.8}N/GaN$ single-QW LDs with well widths L_w=3.6 and 5.4 nm, assuming the partition ratio Q_v=0.33 in panel (a) and Q_v=0.45 in panel (b). J is the total current density, J_{bb} is due to the bb process, and J_0 is calculated without considering the continuous subbands.

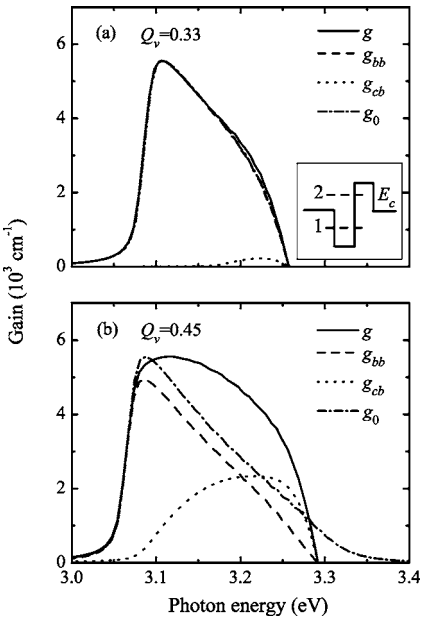

FIG. 3. The gain spectra at threshold for $In_{0.2}Ga_{0.8}N/GaN$ single-QW structures with L_w=3.6 nm, assuming Q_v=0.33 in panel (a) and Q_v=0.45 in panel (b). The spectra g are the total gain, the spectra g_{bb} (g_{cb}) are due to the bb (cb) process, and the g_0 ones are obtained without considering the continuous subbands. Inseted is an illustration of the conduction band profile of the QW with the level of the lowest bound subband edge (level 1) and that of the lowest quasibound subband edge (level 2).

considering the continuous subbands; that is, in calculating J_0 we assume all the carriers to be at the bound subband states. In our calculation, it is found that the current-density components J_{bc} and J_{cc}, involving the valence continuous subbands in the transition processes, are negligibly small compared with the other components J_{bb} and J_{cb}. This is because the density of states of the valence bands is much higher than that of the conduction bands. All the holes hence almost lie in the lowest bound subbands. Therefore we do not show the curves for J_{bc} and J_{cc} in Fig. 2 and henceforth we will not present calculated results concerning transition processes involving the continuous valence subbands. As a result, the difference $J-J_{bb} \simeq J_{cb}$ can reveal the influence of electron spillover into the continuous subbands on the threshold current density. The electron spillover is more prominent as more carriers are injected into the active region. This leads to an increase in the difference $J-J_{bb}$ with the peak gain, as can be seen from the figure. It is also found that the difference $J-J_{bb}$ is larger for larger Q_v since the spillover of electrons is more prominent from a shallower QW. For Q_v=0.45, the difference $J-J_{bb}$ is larger for L_w=5.4 nm in general than for L_w=3.6 nm. Since the currents also depend on the well width, one cannot conclude that the electron spillover is more considerable in a wider well. Contrarily, more percentage of electrons spill from the narrower well for which the bound subband edges are closer to the barrier. It should be noted that for Q_v=0.45 there is an appreciable difference between J and J_0 both for L_w=3.6 nm at threshold (max $g \simeq 5600$ cm^{-1}) and for L_w=5.4 nm at threshold (max $g \simeq 3700$ cm^{-1}). This means that one may obtain an incorrect threshold current without the electron spillover effect taken into account and also may have a misunderstanding of the carrier distribution both in energy and in space. As will be seen later, such an incorrect carrier distribution may cause a significant deviation of gain and spontaneous emission spectra.

To give an insight into the carrier spillover effect on the optical property of QW active regions, we show in Fig. 3 the gain spectra g and their components g_{bb} and g_{cb} at threshold for single-QW structures with L_w=3.6 nm, assuming Q_v=0.33 in panel (a) and Q_v=0.45 in panel (b). For comparison, we also show the gain spectra g_0 which are obtained without considering the carrier spillover. By comparing the curves in both the panels, we find that the electron spillover effect can be neglected for Q_v=0.33, but for Q_v=0.45 the component g_{cb} gives more contribution to the total gain g in the high-energy range, resulting in a broader gain spectrum g, due to a larger number of electrons spilling over to the continuous subband states. The spillover also results in a significant blueshift of the peak gain. However, g_{cb} gives only a small contribution to the peak gain although, as has been seen in Fig. 2(b), the cb process can give a significant current density J_{cb}. There is a qualitative difference between the profiles of the gain spectra g and g_0 for Q_v=0.45. The long tail of the g_0 spectrum for Q_v=0.45 is caused by a broad distribution of electrons in the two-dimensional momentum space.

It should be mentioned that, among the continuous subbands, the lowest quasibound subband and those around it in energy provide the states for electrons that are dominant in the cb transition process. Inseted in Fig. 3(a) is the conduction band profile of the QW with the level of the lowest bound subband edge (level 1) and that of the lowest quasibound subband edge (level 2). The quasibound subband states form a standing wave in the z direction and thus have

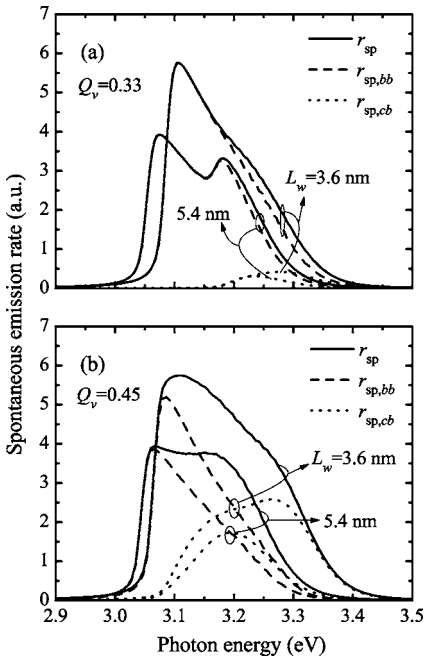

FIG. 4. The spectra of spontaneous emission rates at threshold for $In_{0.2}Ga_{0.8}N/GaN$ single-QW structures with L_w=3.6 and 5.4 nm, assuming Q_v=0.33 in panel (a) and Q_v=0.45 in panel (b). The spectra r_{sp} are the total spontaneous emission rate and the $r_{sp,bb}$ ($r_{sp,cb}$) ones are due to the *bb* (*cb*) process.

a nature of resonance. Because of the resonance nature, the wave functions of the quasibound subbands and their neighbors are much more localized around the QW than those of other subbands. As a result, these more localized subband states give a much larger interband matrix element $M^{\sigma}_{e,ij}$ than others and hence play a dominant part in the *cb* process.

The *cb* process can also cause broadening of the spontaneous emission spectrum. Figure 4 shows the spectra r_{sp} of the total spontaneous emission rate and their components $r_{sp,bb}$ and $r_{sp,cb}$ at threshold for single-QW structures with L_w=3.6 and 5.4 nm, similarly assuming Q_v=0.33 in panel (a) and Q_v=0.45 in panel (b). As expected, the spectra r_{sp} are broader for Q_v=0.45 compared to those for Q_v=0.33 because of more contribution from $r_{sp,cb}$ for the shallower electron QW. For the narrower QW (L_w=3.6 nm) the numbers of carriers needed for threshold are larger, giving the higher and broader spectra r_{sp}. It can be found that there is a subordinate peak at photon energy of 3.18 eV in $r_{sp,bb}$ (and r_{sp}) for Q_v=0.33 and L_w=5.4 nm. No distinct subordinate peak is found in the other $r_{sp,bb}$ spectra. Such a subordinate peak is caused mainly by the optical transition from the second bound conduction subband which does not exist in the other QW structures.

As is well known, for QW lasers the threshold current density J increases as the well width L_w decreases in the range of small well width. This is because the number of carriers needed for threshold increases superlinearly with decreasing L_w. On the other hand, in the range of large well width, the threshold current also increases with increasing L_w because of the wide active region for carrier recombination. As a result, one expects a minimum value of J in the $J-L_w$ curve at an optimum L_w. Nevertheless, the carrier spillover

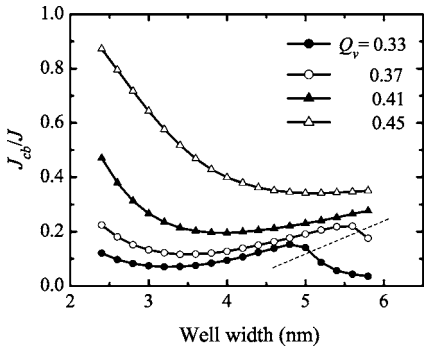

FIG. 5. The ratio J_{cb}/J for $In_{0.2}Ga_{0.8}/GaN$ single-QW LDs at threshold vs the well width L_w with Q_v as a variable parameter (Q_v=0.33, 0.37, 0.41, and 0.45). The dashed line indicates the boundary across which the lowest quasibound subband changes to a bound subband.

makes the situation more complicated. To see this, we show in Fig. 5 the ratio J_{cb}/J at threshold versus the well width L_w with Q_v as a variable parameter. Such a J_{cb}/J ratio can be considered as a measure of the electron spillover to the continuous subbands. As expected, the spillover (and thus the ratio J_{cb}/J) is more serious for larger Q_v. For a small well width, the spillover is more sensitive to the variation of Q_v when Q_v is larger (for a shallower electron QW). As L_w increases from a small value (2.4 nm), each of the ratios J_{cb}/J first decreases to a local minimum and then goes up. The decrease of J_{cb}/J with increasing L_w is caused by the increase of the optical confinement factor Γ that reduces the carrier density needed for threshold and then alleviates the spillover of electrons to the continuous subbands. However, with increasing L_w, the lowest quasibound subband moves downward and the separation decreases between the bound and the lowest quasibound subbands. This increases the electron spillover to the lowest quasibound subband and its neighbors. The interplay of the two counteractive effects causes the curves of J_{cb}/J to go down and then up with increasing L_w until the lowest quasibound subband has its edge below the barriers in energy and becomes the highest bound subband. Around the critical point at which the subband changes from a quasibound to a bound nature, J_{cb}/J reaches a local maximum, as shown in the curves for Q_v=0.33 and 0.37 in Fig. 5. To the right of the dashed line in the figure, the second bound subband appears and the curves again go down and then up, governed by the variations of the confinement factor Γ and the position of the new lowest quasibound subband. Such going down and then up of J_{cb}/J continues as the L_w increases. Finally, as $L_w \to \infty$, $J_{cb}/J \to 0$ which is the value for a three-dimensional active region.

It can be found from Fig. 5 that the *cb* process may become dominant in the optical properties of the QW structures if L_w becomes small for a large Q_v. This situation should be avoided to take advantage of low threshold in a two-dimensional QW.

Figure 6 shows the current densities J and J_{bb} at threshold as a function of L_w for Q_v=0.33 and 0.45. Now we can figure out the variations of the curves with the aid of the explications for Fig. 5. We can take a QW of width in the range of 3–5 nm for Q_v=0.33 and in the range of 4–6 nm for Q_v=0.45 for a low threshold. From the viewpoint of de-

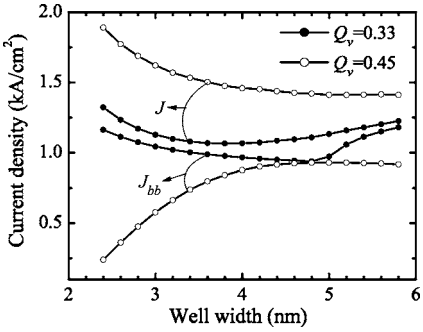

FIG. 6. The current densities J and J_{bb} for $In_{0.2}Ga_{0.8}/GaN$ single-QW LDs at threshold as a function of L_w for Q_v=0.33 and 0.45.

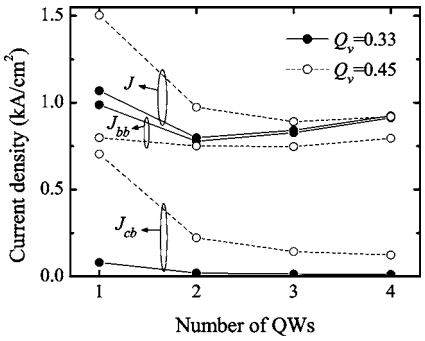

FIG. 8. The current densities J, J_{bb}, and J_{cb} of $In_{0.2}Ga_{0.8}N/GaN$ multi-QW LDs at threshold vs the number of QWs for Q_v=0.33 and 0.45.

vice design, such wide ranges of well width can allow a freedom of choosing a desired emission wavelength from a wide spectral range. As expected, we find a minimum of J_{bb} and a local maximum of $J_{cb}=J-J_{bb}$ for $Q_v=0.33$ at $L_w=4.8$ nm around which the lowest quasibound subband changes to the highest bound subband.

The carrier spillover depends also on the cavity loss α that determines the carrier density required for threshold. Figure 7 shows the ratio J_{cb}/J at threshold versus the well width L_w for $Q_v=0.33$ and 0.45 with α as a variable parameter. As the figure shows, the spillover can be significantly reduced by decreasing the cavity loss α. This implies that a long cavity is preferred to alleviate the spillover effect, especially when Q_v is large.

As has been pointed out, the carrier spillover and the threshold current can be significantly reduced by increasing the well width L_w for a large Q_v. However, this will cause redshift in the emission wavelength and may sacrifice the purpose of short-wavelength emission. To reduce the electron spillover and simultaneously keep a short-wavelength emission, one can employ a structure of multiple QWs. Figure 8 shows the current densities J, J_{bb}, and J_{cb} at threshold versus the number of QWs in the active region for $Q_v=0.33$ and 0.45. The width of each QW is fixed at $L_w=3.6$ nm. As can be seen, the current density J_{cb} is considerably reduced for $Q_v=0.45$ as the QW number increases from 1 to 2. Consequently, this causes a considerable reduction of the total threshold current density J for $Q_v=0.45$. As the QW number changes from 2 to 3, there is a slight reduction in J_{cb} but no appreciable change in J_{bb} for $Q_v=0.45$.

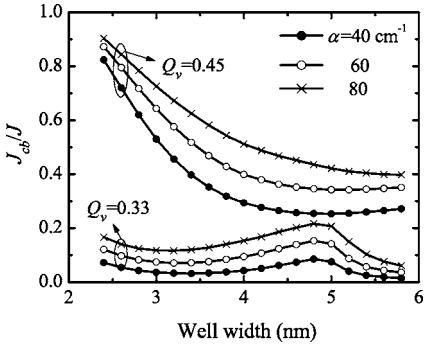

FIG. 7. The ratio J_{cb}/J for $In_{0.2}Ga_{0.8}/GaN$ single-QW LDs at threshold vs the well width L_w for $Q_v=0.33$ and 0.45 with the cavity loss α as a variable parameter (α=40, 60, and 80 cm^{-1}).

Further increasing the QW number does not significantly reduce J_{cb} but causes an increase of J_{bb}, implying that a triple-QW structure is preferred for a low threshold when $Q_v=0.45$. For $Q_v=0.33$, a double-QW structure seems preferred for low threshold.

Finally, it is worthwhile to make clear the influence of temperature variation on the electron spillover since the heat dissipation is still a critical issue for the nitride LDs. The rise in temperature causes a broadening of carrier distribution in energy. Therefore, we also expect spectral broadening in the gain g and the spontaneous emission rate r_{sp} with the temperature rising. This can be seen from Fig. 9, which is the plot of the g and the r_{sp} spectra of 3.6 nm single-QW structures at two different temperatures T=300 and 400 K for (a) $Q_v=0.33$ and (b) $Q_v=0.45$. The broadness of the spectra for $Q_v=4.5$ at T=400 K in Fig. 9(b) means that the electron spillover is more serious at higher temperature when the QW is shallow.

Figure 10 shows the various current densities at threshold as functions of temperature T for the 3.6 nm single-QW

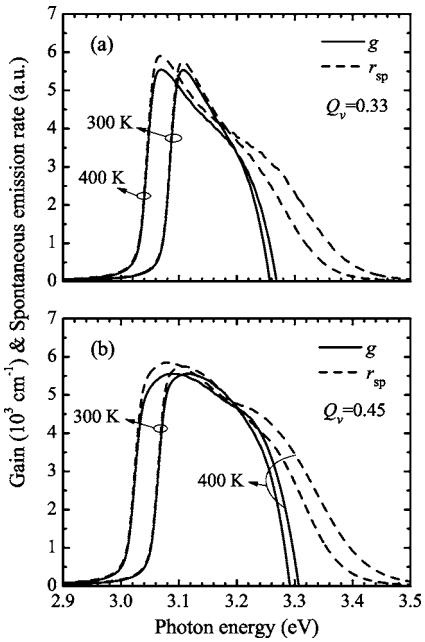

FIG. 9. The spectra of the gain g and the spontaneous emission rate r_{sp} at two different temperatures T=300 and 400 K for 3.6 nm $In_{0.2}Ga_{0.8}N/GaN$ single-QW LDs at threshold with (a) $Q_v=0.33$ and (b) $Q_v=0.45$.

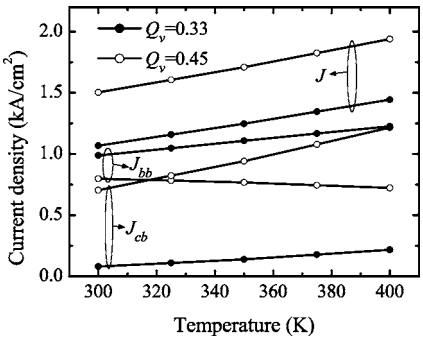

FIG. 10. The current densities J, J_{bb}, and J_{cb} at threshold as functions of temperature T for the 3.6 nm $In_{0.2}Ga_{0.8}/GaN$ single-QW LDs with Q_v =0.33 and 0.45.

structures with Q_v=0.33 and 0.45. With rising T, the J_{cb} at threshold increases more for Q_v=0.45 than for Q_v=0.33 due to a smaller separation between the lowest quasibound and the true bound subbands for the shallower QW. Quite differently, the J_{bb} decreases for Q_v=0.45 but increases for Q_v =0.33 with rising T. This can be understood by the fact that the distribution probability function becomes flatter for a higher T and that the density of states around the quasibound subband edge is much larger than that of the bound subband. As a result, the electron density in the bound subband at threshold decreases for the shallow QW as T rises. However, the increase of the J_{bb} with rising T for the deep QW is due to the gain spectrum broadening that requires a high carrier density at threshold. It is noticed that for Q_v=0.45 the J_{cb} becomes dominant over the J_{bb} as $T>320$ K, implying that the optical property of the shallow QWs is no longer of pure two-dimensional nature. For deep QWs, the spillover is not serious in the range of T=300–400 K.

In this study, we have taken the valence band partition ratio Q_v as a variable parameter because of lack of a compelling value for this parameter. However, in the true case, Q_v must be fixed. It may be 0.33, or 0.45, or more probably another value. Recent published works have come to an agreement that the value of Q_v is small (close to 0.3).[21,22] Even for the small value, the spillover effect is not negligible on the threshold current. Nevertheless, regardless of the value of Q_v, our present work has introduced the important concept of carrier spillover, applicable not only to the nitride LDs but also to other kinds of LDs such as short-wavelength AlGaInP/GaAs LDs.

We have presented the calculated results by assuming quasiequilibrium for electrons in the conduction band and for holes in the valence band. This means that our calculations are applicable to the case at and below threshold. Above threshold, the high interband transition rate makes the assumption of quasiequilibrium no longer the case. It causes the spectral hole burning of the distribution function, which may have a reduction of the electron population in the bound subbands and meanwhile an increase of the population in the continuous subbands. Consequently, we expect a sublinear L-I relation above threshold.

IV. CONCLUSION

The influences of spillover effects on radiative current density, gain spectra, and spontaneous emission spectra in InGaN/GaN QW LDs have been theoretically studied in detail. To this end, the continuous subbands above the barriers in energy are considered for the spillover electrons. It has been shown that there are obvious differences in the radiative current densities and gain spectra between the cases with and without considering the spillover effect. It is shown that the spillover effects are important, especially to shallow QWs. The participation of spillover electrons in interband transitions causes spectral broadening of the gain and the spontaneous emission and hence increases the threshold current. Such effects become more serious as the cavity loss increases or the temperature rises. To reduce the spillover, one can employ a multi-QW structure for the LDs. The concept of electron spillover is important not only to the nitride LDs but also to other kinds of LDs that have a shallow QW and large asymmetry in density of states between the conduction and the valence bands.

ACKNOWLEDGMENTS

This work was supported by the National Science Council under Grant No. 95-2221-E-009-281 and MOE ATU Program of Republic of China.

[1]T. Yamaguchi, Y. Ueda, Y. Matsushita, K. Koga, and T. Niina, Optoelectron., Devices Technol. **7**, 57 (1992).
[2]W. Xie, D. C. Grillo, R. L. Gunshor, M. Kobayashi, H. Jeon, J. Ding, A. V. Nurmikko, G. C. Hua, and N. Otsuka, Appl. Phys. Lett. **60**, 1999 (1992).
[3]D. E. Eason, Z. Yu, W. C. Hughes, W. H. Roland, C. Boney, J. W. Cook, Jr., J. F. Schetzina, G. Cantwell, and W. C. Harasch, Appl. Phys. Lett. **66**, 115 (1995).
[4]J. I. Pankove, E. A. Miller, and J. E. Berkeyheiser, RCA Rev. **32**, 383 (1971).
[5]S. T. Yen and C. P. Lee, IEEE J. Quantum Electron. **33**, 443 (1997).
[6]S. Strite and H. Morkoç, J. Vac. Sci. Technol. B **10**, 1237 (1992).
[7]H. Morkoç, S. Strite, G. B. Gao, M. E. Lin, B. Sverdlov, and M. Burns, J. Appl. Phys. **76**, 1363 (1994).
[8]S. Nakamura, M. Senoh, S. Nagahama, N. Iwasa, T. Yamada, T. Matsushita, Y. Sugimoto, and H. Kiyoku, Appl. Phys. Lett. **69**, 1568 (1996).
[9]J. Y. Chang and Y. K. Kuo, J. Appl. Phys. **93**, 4992 (2003).
[10]M. Hansen, J. Piprek, P. M. Pattison, J. S. Speck, S. Nakamura, and S. P. Denbaars, Appl. Phys. Lett. **81**, 4275 (2002).
[11]S. N. Lee, S. Y. Cho, H. Y. Ryu, J. K. Son, H. S. Paek, T. Sakong, T. Jang, K. K. Choi, K. H. Ha, M. H. Yang, O. H. Nam, Y. Park, and E. Yoon, Appl. Phys. Lett. **88**, 111101-1 (2006).
[12]S. P. Łepkowski and S. Krukowski, J. Appl. Phys. **100**, 016103-1 (2006).
[13]G. Martin, A. Botchkarev, A. Rockett, and H. Morkoç, Appl. Phys. Lett. **68**, 2541 (1996).
[14]F. D. Sala, A. D. Carlo, P. Lugli, F. Bernardini, V. Fiorentini, R. Scholz, and J. M. Jancu, Appl. Phys. Lett. **74**, 2002 (1999).
[15]G. Franssen, T. Suski, and P. Perlin, Appl. Phys. Lett. **87**, 041109 (2005).
[16]S. L. Chuang and C. S. Chang, Phys. Rev. B **54**, 2491 (1996).
[17]F. Mireles and S. E. Ulloa, Phys. Rev. B **60**, 13659 (1999).
[18]S. T. Yen, Phys. Rev. B **66**, 075340 (2002).
[19]S. L. Chung, IEEE J. Quantum Electron. **32**, 1791 (1996).
[20]I. Vurgaftman and J. R. Meyer, J. Appl. Phys. **94**, 3675 (2003).
[21]S. H. Wei and A. Zunger, Appl. Phys. Lett. **69**, 2719 (1996).
[22]C. Manz, M. Kunzer, H. Obloh, A. Ramakrishnan, and U. Kaufmann, Appl. Phys. Lett. **74**, 3993 (1999).